ISSN 1007-9327 (print)
ISSN 2219-2840 (online)

World Journal of *Gastroenterology*

World J Gastroenterol 2022 June 28; 28(24): 2636-2781

Published by Baishideng Publishing Group Inc

World Journal of Gastroenterology

Contents

Weekly Volume 28 Number 24 June 28, 2022

REVIEW

MINIREVIEWS

ORIGINAL ARTICLE

Basic Study

Clinical and Translational Research

Retrospective Cohort Study

Retrospective Study

Observational Study

LETTER TO THE EDITOR

ABOUT COVER

Editorial Board Member of *World Journal of Gastroenterology*, Vasiliy Ivanovich Reshetnyak, DSc, MD, Full Professor, Department of Propaedeutic of Internal Diseases and Gastroenterology, A.I. Yevdokimov Moscow State University of Medicine and Dentistry, p. 1, 20 Delegatskaya Street, Moscow 127473, Russia. vasiliy.reshetnyak@yandex.ru

AIMS AND SCOPE

The primary aim of *World Journal of Gastroenterology* (*WJG*, *World J Gastroenterol*) is to provide scholars and readers from various fields of gastroenterology and hepatology with a platform to publish high-quality basic and clinical research articles and communicate their research findings online. *WJG* mainly publishes articles reporting research results and findings obtained in the field of gastroenterology and hepatology and covering a wide range of topics including gastroenterology, hepatology, gastrointestinal endoscopy, gastrointestinal surgery, gastrointestinal oncology, and pediatric gastroenterology.

INDEXING/ABSTRACTING

The *WJG* is now indexed in Current Contents®/Clinical Medicine, Science Citation Index Expanded (also known as SciSearch®), Journal Citation Reports®, Index Medicus, MEDLINE, PubMed, PubMed Central, and Scopus. The 2021 edition of Journal Citation Report® cites the 2020 impact factor (IF) for *WJG* as 5.742; Journal Citation Indicator: 0.79; IF without journal self cites: 5.590; 5-year IF: 5.044; Ranking: 28 among 92 journals in gastroenterology and hepatology; and Quartile category: Q2. The *WJG*'s CiteScore for 2020 is 6.9 and Scopus CiteScore rank 2020: Gastroenterology is 19/136.

RESPONSIBLE EDITORS FOR THIS ISSUE

Production Editor: *Yu-Xi Chen*; **Production Department Director:** *Xu Guo*; **Editorial Office Director:** *Ze-Mao Gong*.

NAME OF JOURNAL
World Journal of Gastroenterology

ISSN
ISSN 1007-9327 (print) ISSN 2219-2840 (online)

LAUNCH DATE
October 1, 1995

FREQUENCY
Weekly

EDITORS-IN-CHIEF
Andrzej S Tarnawski

EDITORIAL BOARD MEMBERS
http://www.wjgnet.com/1007-9327/editorialboard.htm

PUBLICATION DATE
June 28, 2022

INSTRUCTIONS TO AUTHORS
https://www.wjgnet.com/bpg/gerinfo/204

GUIDELINES FOR ETHICS DOCUMENTS
https://www.wjgnet.com/bpg/GerInfo/287

GUIDELINES FOR NON-NATIVE SPEAKERS OF ENGLISH
https://www.wjgnet.com/bpg/gerinfo/240

PUBLICATION ETHICS
https://www.wjgnet.com/bpg/GerInfo/288

PUBLICATION MISCONDUCT
https://www.wjgnet.com/bpg/gerinfo/208

ARTICLE PROCESSING CHARGE
https://www.wjgnet.com/bpg/gerinfo/242

STEPS FOR SUBMITTING MANUSCRIPTS
https://www.wjgnet.com/bpg/GerInfo/239

ONLINE SUBMISSION
https://www.f6publishing.com

World Journal of Gastroenterology

Submit a Manuscript: https://www.f6publishing.com

World J Gastroenterol 2022 June 28; 28(24): 2733-2747

DOI: 10.3748/wjg.v28.i24.2733

ISSN 1007-9327 (print) ISSN 2219-2840 (online)

ORIGINAL ARTICLE

Retrospective Study

Radiomic analysis based on multi-phase magnetic resonance imaging to predict preoperatively microvascular invasion in hepatocellular carcinoma

Yue-Ming Li, Yue-Min Zhu, Lan-Mei Gao, Ze-Wen Han, Xiao-Jie Chen, Chuan Yan, Rong-Ping Ye, Dai-Rong Cao

Specialty type: Gastroenterology and hepatology

Provenance and peer review: Unsolicited article; Externally peer reviewed.

Peer-review model: Single blind

Peer-review report's scientific quality classification

Grade A (Excellent): 0
Grade B (Very good): B
Grade C (Good): C, C, C
Grade D (Fair): 0
Grade E (Poor): 0

P-Reviewer: Li L, New Zealand; Shomura M, Japan; Suda T, Japan

Received: December 24, 2021
Peer-review started: December 24, 2021
First decision: March 10, 2022
Revised: March 20, 2022
Accepted: May 12, 2022
Article in press: May 12, 2022
Published online: June 28, 2022

Yue-Ming Li, Yue-Min Zhu, Lan-Mei Gao, Ze-Wen Han, Xiao-Jie Chen, Chuan Yan, Rong-Ping Ye, Dai-Rong Cao, Department of Radiology, The First Affiliated Hospital of Fujian Medical University, Fuzhou 350005, Fujian Province, China

Yue-Ming Li, Key Laboratory of Radiation Biology (Fujian Medical University), Fujian Province University, Fuzhou 350005, Fujian Province, China

Corresponding author: Dai-Rong Cao, MD, Chief Doctor, Department of Radiology, The First Affiliated Hospital of Fujian Medical University, No. 20 Chazhong Road, Fuzhou 350005, Fujian Province, China. 3502505836@qq.com

Abstract

BACKGROUND

The prognosis of hepatocellular carcinoma (HCC) remains poor and relapse occurs in more than half of patients within 2 years after hepatectomy. In terms of recent studies, microvascular invasion (MVI) is one of the potential predictors of recurrence. Accurate preoperative prediction of MVI is potentially beneficial to the optimization of treatment planning.

AIM

To develop a radiomic analysis model based on pre-operative magnetic resonance imaging (MRI) data to predict MVI in HCC.

METHODS

A total of 113 patients recruited to this study have been diagnosed as having HCC with histological confirmation, among whom 73 were found to have MVI and 40 were not. All the patients received preoperative examination by Gd-enhanced MRI and then curative hepatectomy. We manually delineated the tumor lesion on the largest cross-sectional area of the tumor and the adjacent two images on MRI, namely, the regions of interest. Quantitative analyses included most discriminant factors (MDFs) developed using linear discriminant analysis algorithm and histogram analysis with MaZda software. Independent significant variables of clinical and radiological features and MDFs for the prediction of MVI were estimated and a discriminant model was established by univariate and

multivariate logistic regression analysis. Prediction ability of the above-mentioned parameters or model was then evaluated by receiver operating characteristic (ROC) curve analysis. Five-fold cross-validation was also applied *via* R software.

RESULTS

The area under the ROC curve (AUC) of the MDF (0.77-0.85) outperformed that of histogram parameters (0.51-0.74). After multivariate analysis, MDF values of the arterial and portal venous phase, and peritumoral hypointensity in the hepatobiliary phase were identified to be independent predictors of MVI ($P < 0.05$). The AUC value of the model was 0.939 [95% confidence interval (CI): 0.893-0.984, standard error: 0.023]. The result of internal five-fold cross-validation (AUC: 0.912, 95%CI: 0.841-0.959, standard error: 0.0298) also showed favorable predictive efficacy.

CONCLUSION

Noninvasive MRI radiomic model based on MDF values and imaging biomarkers may be useful to make preoperative prediction of MVI in patients with primary HCC.

Key Words: Hepatocellular carcinoma; Microvascular invasion; Magnetic resonance imaging; Radiomic analysis; Imaging biomarkers

Core Tip: We developed a radiomic analysis model based on pre-operative magnetic resonance imaging data to predict microvascular invasion (MVI) in hepatocellular carcinoma (HCC). Quantitative analyses included most discriminant factors (MDFs) developed using the linear discriminant analysis algorithm and histogram analysis with MaZda software. The area under the receiver operating characteristic curve value of the model and the result of internal five-fold cross-validation showed favorable predictive efficacy. Noninvasive radiomic model based on MDF values and imaging biomarkers may be useful to make preoperative prediction of MVI in patients with primary HCC.

Citation: Li YM, Zhu YM, Gao LM, Han ZW, Chen XJ, Yan C, Ye RP, Cao DR. Radiomic analysis based on multi-phase magnetic resonance imaging to predict preoperatively microvascular invasion in hepatocellular carcinoma. *World J Gastroenterol* 2022; 28(24): 2733-2747

URL: https://www.wjgnet.com/1007-9327/full/v28/i24/2733.htm

DOI: https://dx.doi.org/10.3748/wjg.v28.i24.2733

INTRODUCTION

As important therapies for hepatocellular carcinoma (HCC), liver resection and transplantation are widely applied in clinic and the techniques have great advances. However, the prognosis remains poor and relapse occurs in more than half patients within 2 years after hepatectomy[1]. In terms of recent studies, microvascular invasion (MVI) is one of the potential predictors of recurrence[2,3]. MVI, only seen under the microscope, is defined as the appearance of tumor cells in smaller vessels inside the liver which include small portal vein and small lymphatic vessels or hepatic artery[4,5]. And MVI can be classified as four subclasses varying from M0 to M3, and higher grade usually indicates higher invasiveness of HCC and poorer survival rate[6]. Nonetheless, MVI is diagnosed by post-surgery histological result at present, which is the gold standard. The accurate prediction of MVI before operation can help achieve the anatomic resection with expanding resection margin even for a small tumor[7]. Thus, accurate preoperative prediction of MVI is potentially beneficial to the optimization of treatment planning[3,8].

There have been some studies to preoperatively predict MVI in terms of serum markers, radiological features, or imaging techniques[9-11]. For example, albumin was independently associated with MVI [9]. Besides, non-smooth tumor margins had strong diagnostic power and were of great importance for MVI assessment[10]. Moreover, gadolinium ethoxybenzyl-diethylenetriaminepentaacetic acid (Gd-EOB-DTPA), a special hepatocellular parenchymal contrast agent for magnetic resonance imaging (MRI), was valuable for MVI prediction as well[11,12]. However, the levels of serum markers are instable and likely to be affected by other diseases, and the imaging characteristics are evaluated subjectively and lack of conformance between observers. Thus, a more reliable biomarker is needed for preoperative prediction of MVI.

Quantitative analysis may have advantages over subjective analysis in reflecting valuable microscopic image features. Radiomic analysis can quantify the spatial variations in gray-level patterns, image spectral properties, and pixel interrelationships, which therefore has attracted great interest[13-15]. Using automation algorithms based on big data and with the advantages of noninvasiveness, radiomics analysis provides a powerful tool for modern medicine, and it can broadly combine multiple biomarkers and then guide clinical decision-making for patients suspected with cancer[16]. Various machine-learning methods have been used for radiomic analysis for MVI prediction, such as support vector machine and random forest[17,18]. To the best of our knowledge, there is not yet radiomics study based on linear discriminant analysis (LDA) algorithm to predict MVI. Additionally, even without spatial information, histogram analysis alone can indicate a gray-level distribution and is used for MVI prediction[19,20].

Our aim was to identify the histogram parameters alone that are predictive for MVI, and determined the prediction capacity of LDA radiomic models based on multiple phases in pre-operative Gd-enhanced MRI alone or combined with the image features for detecting MVI.

MATERIALS AND METHODS

Patients

Patients who underwent Gd-enhanced MRI examination before surgery were consecutively recruited between June 2019 and November 2021. The inclusion criteria were: (1) Solitary HCC lesion which was resectable or multiple HCC lesions appearing within one liver lobe; (2) No macroscopic vascular invasion; (3) Received the examination of Gd-enhanced MRI of the liver [with or without hepatobiliary phase (HBP)] within 1 mo before surgery; (4) Received curative hepatectomy; and (5) Verification of MVI by pathological evidence. The exclusion criteria were as follows: (1) Other anti-tumor therapies had been performed before surgery; (2) Pathological or clinical information was incomplete; (3) Imaging was not enough for analysis as a result of motion artifact; and (4) MRI performed in a different 3.0T MR machine. A total of 113 patients (91 men and 22 women; age ranging from 29–88 years, median age 58 years old) were included. According to pathologic results, HCC patients were allocated into MVI-positive (MVI+) and MVI-negative (MVI-) groups. The inclusion and exclusion criteria are shown in the flow diagram (Figure 1). This single-center retrospective cohort study was approved by the Institutional Review Board (No. [2019]283), and the requirement for informed consent was waived.

MRI examination

A 3.0T MR machine (MAGNETOM Verio; Siemens, Healthcare, Erlangen, Germany) with a dedicated phased-array body coil was used for MRI. The standard abdominal MRI protocol included: (1) Axial T2-weighted fat-suppressed turbo-spin-echo: Repetition time (TR)/echo time (TE), 4700/79 msec, slice thickness, 5 mm, slice gap, 1 mm, FOV, 21 mm × 38 mm; (2) In-phase and out-of-phase axial T1-weighted imaging (T1WI): TR/TE, 133/2.5 msec (in-phase), 6.2 msec (out-phase), slice thickness, 5 mm, slice gap, 1 mm, FOV, 21 mm × 38 mm; (3) Diffusion-weighted imaging (b = 50, 800 sec/mm^2) performed using a free-breathing single-shot echo-planar technique, TR/TE, 9965/73 msec, slice thickness, 5 mm, slice gap, 1 mm, FOV, 21 mm × 38 mm. The MRI system automatically calculated the corresponding ADC maps; and (4) Contrast enhanced MRI: A 3D gradient echo sequence with volumetric interpolated breath-hold examination was performed before and after injection of gadobenate dimeglumine (MultiHance; Bracco) at a dose of 0.2 mL/kg and at a rate of 2 mL/sec followed by a 20 mL saline flush with the following parameters: TR/TE, 3.9/1.4 msec, slice thickness 3 mm, slice gap, 0.6 mm, FOV, 25 mm × 38 mm. Hepatic arterial phase (AP), portal venous phase (PVP), equilibrium phase (EP), and HBP images were obtained at 20–30 sec, 70–80 sec, 180 sec, and 90 min after contrast medium injection, respectively.

Radiomic analysis

MaZda software (version 4.6.0, available at http://www.eletel.p.lodz.pl/mazda/) was used for radiomic analysis[21], and Digital Imaging Transformation and Communications in Medicine (DICOM) format was needed for compatibility with MaZda software. Images (MVI+ and MVI-) were loaded into the MaZda software; then, regions of interest (ROIs) were segmented manually by one radiologist, on the largest cross-sectional area and adjacent two images of the tumor or largest lesion (in the case of multiple lesions), which also included cystic necrotic regions. To delineate the tumor, the reference was based on HBP or T2-weighted imaging (T2WI) (in the case of artifact) images which were first segmented. Subsequently, the ROI was overlaid onto other phase images as required. If the respiratory movement caused the change of tumor location, the ROI was finely adjusted.

Radiomic analysis was performed with the MaZda package after loading all segmented tumor T2WI and T1WI + Gd images; within each ROI, 101 features were generated. Six different statistical image descriptors including gradient features, histogram features, gray level co-occurrence matrix, gray level run-length matrix, wavelet transform, and autoregressive model were used to create these radiomic features[21,22]. In each ROI, gray-level was normalized to minimize the effect of brightness and contrast

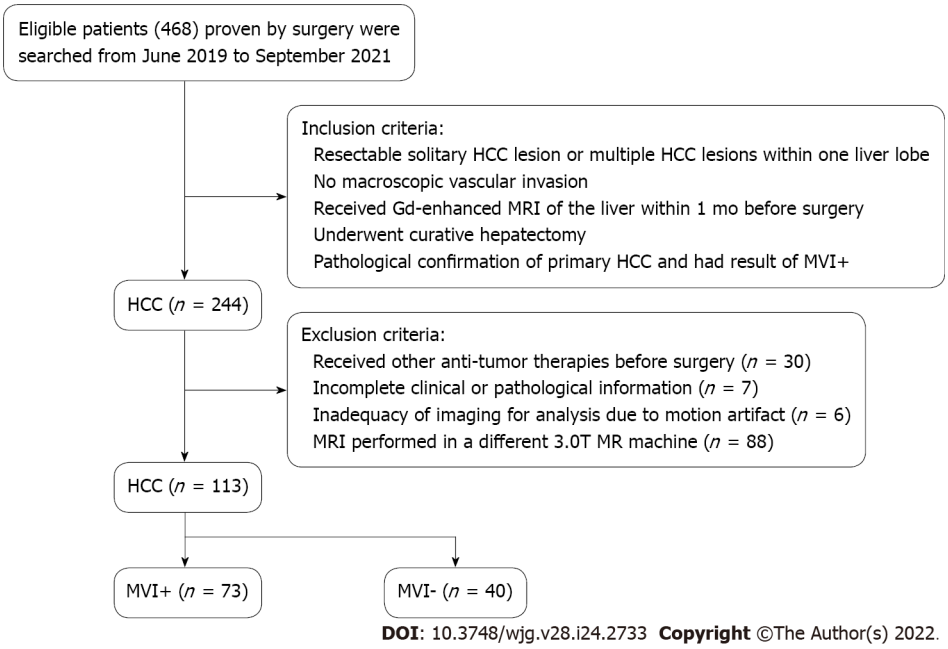

Figure 1 Flowchart of study selection process. HCC: Hepatocellular carcinoma; MVI: Microvascular invasion.

variation by image intensities in the range μ ± 3σ (μ, gray-level mean; σ, standard deviation), and the range was quantized to 6 bits/pixel[23,24].

Dimension reduction is necessary because it is impractical for clinicians to analyze all radiomic features on each patient and curse of dimensionality may happen in the case of too many features. Thus, the useful features were selected among 101 features in each sequence using algorithms, *i.e.*, mutual information (MI), Fisher coefficient (Fisher), and probability of classification error and average correlation coefficients (POE + ACC). These algorithms were used to select 30 highest discriminative power features in each sequence for further analysis. The statistical B11 radiomic analysis package (a plug-in of Mazda software) was used for analyzing these 30 features. A LDA model with the lowest misclassification rate was used to calculate the most discriminant factor (MDF)[25], which served as a comprehensive variable for discrimination and represented a linear transformation of these input 30 features that achieved the maximum separation for samples the between MVI+ and MVI- groups and the minimum separation of samples within each group. Hence, there were six MDFs, *i.e.*, MDF_{T1WI}, MDF_{T2WI}, MDF_{AP}, DMF_{PVP}, MDF_{EP}, and MDF_{HBP}.

The values of the nine histogram features (mean, variance, skewness, kurtosis, percent 1%, percent 10%, percent 50%, percent 90% and percent 99%) previously described (*i.e.*, one of six different statistical image descriptors used for radiomic analysis) were separately saved in addition for the comparison with MDF values. All characteristics of radiomic analysis were generated as presented in Figures 2 and 3.

Analysis of semantic features

In each case, an optimal window setting was adjusted to evaluate the preoperative MR images in the Picture Archiving and Communication System. The imaging features for each HCC were evaluated by two abdominal radiologists independently based on the following criteria: (1) Arterial rim enhancement, defined based on the image with irregular ring-like enhancement with relatively hypovascular central areas in the AP[26,27]; (2) Arterial peritumoral enhancement, defined based on the detectable crescent or polygonal shaped enhancement outside the tumor margin, which broadly contact with the tumor border in the AP, changing to isointense with liver parenchyma background in the delayed phase [28]; (3) Tumor margin, also defined as smooth margin, with the representative image being nodular tumors with smooth contour, or non-smooth margin presenting as non-nodular tumors with irregular margin that had surrounding budding portion in the transverse and coronal HBP images[10,28]; (4) Radiological capsule, presenting as peripheral edge of smooth hyperenhancement in the portal venous or EP[28,29]; (5) Tumor hypointensity in the HBP, shown as lower SI than that of the surrounding liver [12,30]; and (6) Peritumoral hypointensity in the HBP, defined as wedge-shaped or flame-like hypointense area of hepatic parenchyma located outside of the tumor margin in the HBP[31]. Two radiologists assessed the features of the HCC images or the largest lesion (in the case of multiple lesions). The final decision was based on their consensus.

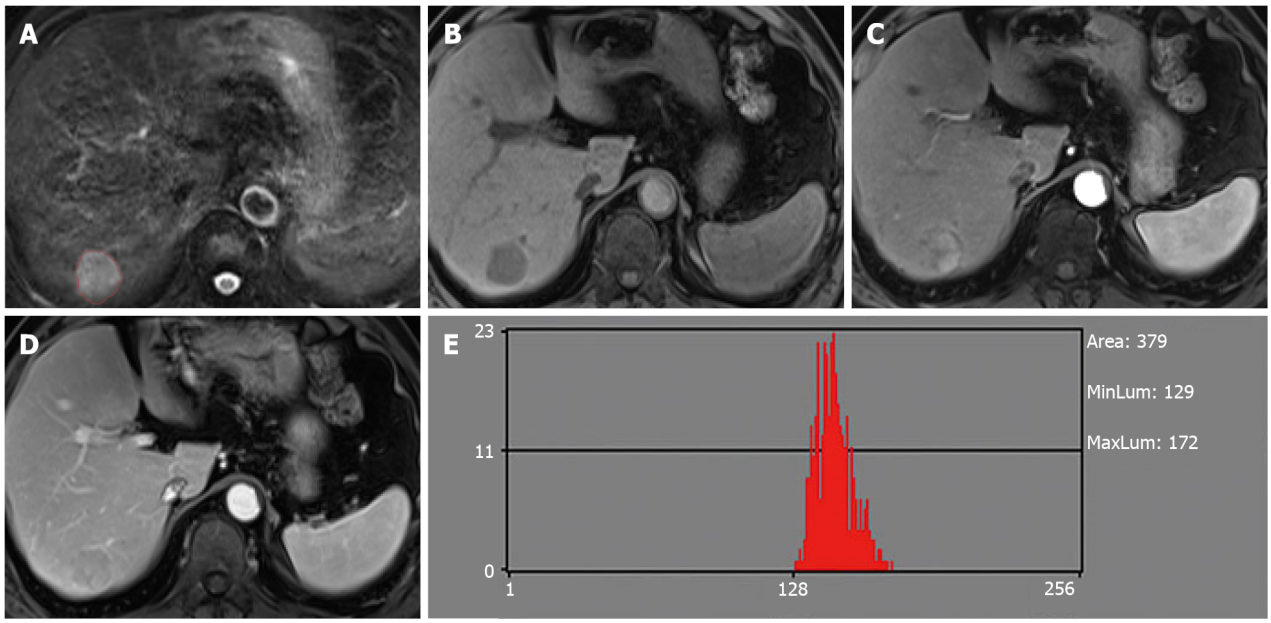

DOI: 10.3748/wjg.v28.i24.2733

Figure 2 Hepatocellular carcinoma without microvascular invasion in a 60-year-old man. A: The lesion showed slightly high signal intensity on T2-weighted imaging (T2WI) and was first regions of interest segmented; B: T1WI showed hypointensity; C: Hyper-enhancement in the arterial phase; D: The lesion showed wash-out in the portal venous phase; E: Histogram map derived from the portal venous phase.

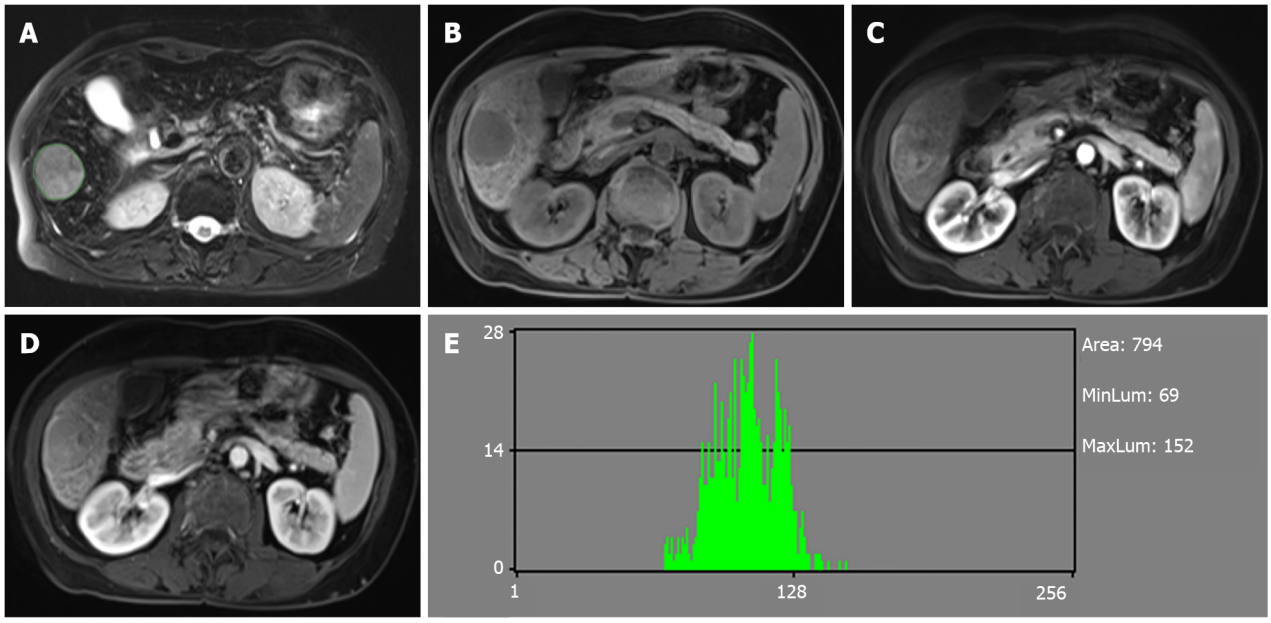

DOI: 10.3748/wjg.v28.i24.2733

Figure 3 Hepatocellular carcinoma with microvascular invasion in a 68-year-old woman. A: The lesion also showed slightly high signal intensity on T2-weighted imaging (T2WI) and was segmented; B: T1WI showed hypointensity; C: Hyper-enhancement in the arterial phase; D: The lesion showed wash-out in the portal venous phase; E: Histogram map derived from the portal venous phase indicating that the parameter of histogram was significantly different between the two groups.

Histopathological analysis

The tumor size, number, and capsule condition were collected and analyzed. The histological type, differentiation grade, lymphocyte infiltration, satellite nodules, MVI status, and chronic liver disease were compared[32]. The definition of MVI was the presence of tumor emboli in an endothelial cells-lined vascular space. The experienced pathologists reported the histopathological results after reviewing the clinical and imaging files.

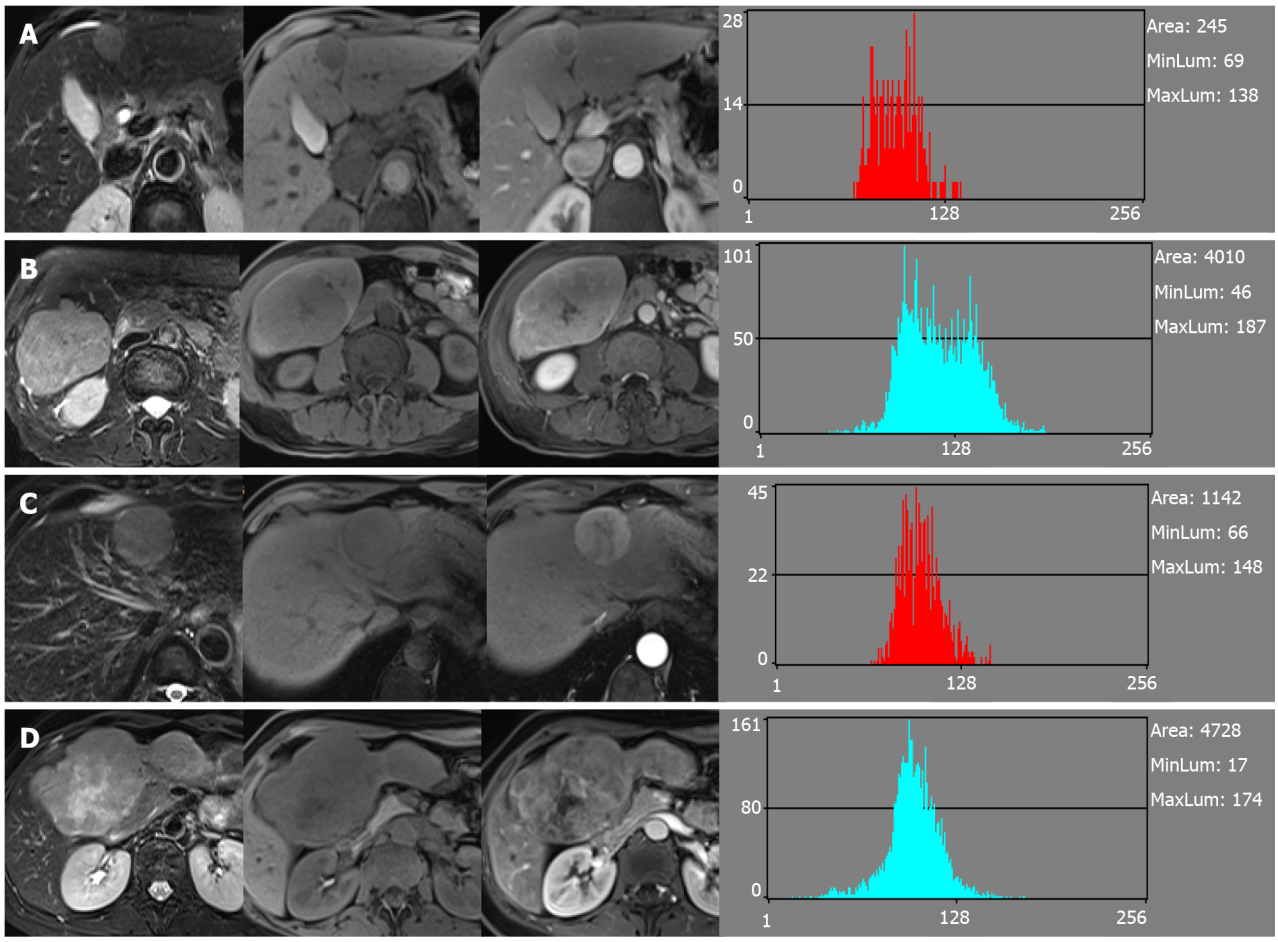

DOI: 10.3748/wjg.v28.i24.2733

Figure 4 Similar histogram features but different most discriminant factors. A: Hepatocellular carcinoma without microvascular invasion and the feature derived from the portal venous phase (PVP); B: Hepatocellular carcinoma with microvascular invasion and features derived from the PVP. Case B showed similar histogram features but different most discriminant factors (MDF) compared with case A; C: Hepatocellular carcinoma without microvascular invasion and features derived from the arterial phase (AP); D: Hepatocellular carcinoma with microvascular invasion and features derived from the AP. Case D showed similar histogram features but different MDF compared with case C.

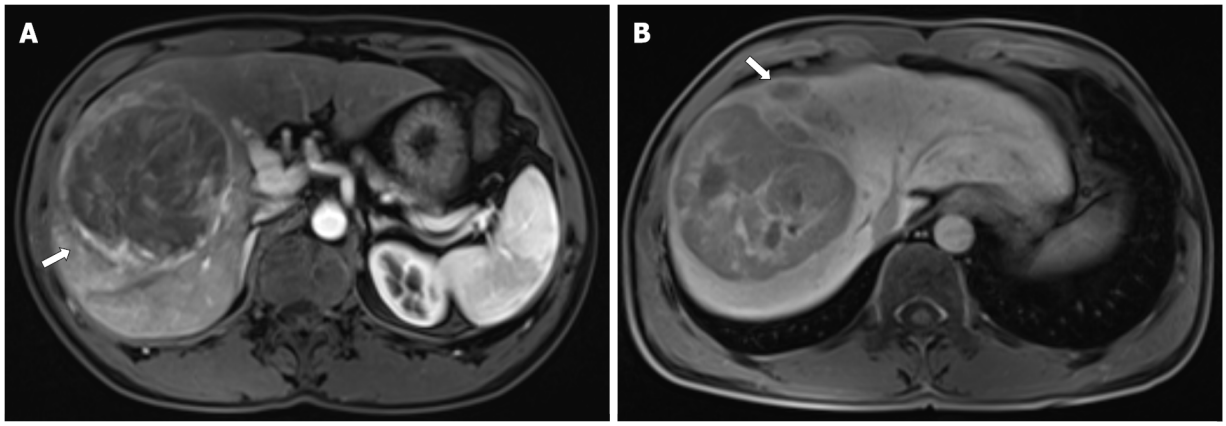

DOI: 10.3748/wjg.v28.i24.2733

Figure 5 Hepatocellular carcinoma with microvascular invasion in a 47-year-old man. A: Gd-enhanced arterial phase magnetic resonance imaging showed arterial rim enhancement (arrow); B: Hepatobiliary phase image showing peritumoral hypointensity (arrow).

Statistical analysis

SPSS for Windows (version 25.0) and Medcalc (Version 15.2.2) were used to generate the receiver operating characteristic (ROC) curves and compare the diagnostic performance for identifying MVI. The

Table 1 Comparison of patient characteristics according to microvascular invasion

Characteristic	MVI+ (*n* = 73)	MVI- (*n* = 40)	*P* value
Age (yr)[1]	56.82 ± 13.38	57.50 ± 11.98	0.790
Gender, *n* (%)			0.374
Male	57 (78.1)	34 (85.0)	
Female	16 (21.9)	6 (15.0)	
Tumor number, *n* (%)			0.152
1	58 (79.5)	36 (90.0)	
≥ 2	15 (20.5)	4 (10.0)	
AFP, *n* (%)			0.023
≤ 20	23 (31.5)	23 (57.5)	
20-400	22 (30.1)	9 (22.5)	
> 400	28 (38.4)	8 (20.0)	
HBsAg, *n* (%)			0.267
Negative	13 (17.8)	4 (10.0)	
Positive	60 (82.2)	36 (90.0)	
Pathologic grade, *n* (%)			0.042
Well	0 (0.0)	1 (2.5)	
Moderate	39 (53.4)	28 (70.0)	
Poor	34 (46.6)	11 (27.5)	
Location, *n* (%)			0.891
Left lobe	21 (28.8)	13 (32.5)	
Right lobe	51 (69.9)	27 (67.5)	
Caudate lobe	1 (1.3)	0 (0.0)	

[1]Data are the mean ± SD.

AFP: Alpha-fetoprotein; HBsAg: Hepatitis B surface antigen; MVI: Microvascular invasion.

areas under the ROC curve (AUCs) were used to assess the predictive efficacy and the optimal cutoff values from the maximum Youden's index were calculated, as well as the corresponding sensitivity and specificity for discriminating between MVI+ and MVI-. Univariate and multivariate logistic regression analyses were performed to confirm the significant variables related to MVI including clinical factors, imaging features, and MDFs in different sequences, and then build a discriminant model. Multivariate logistic regression analysis was performed using forward stepwise elimination method to identify the independent predictors. The prediction ability of significant MDF and the discriminant model was evaluated by AUC. Five-fold cross-validation was performed using the "caret" package, and nomogram was used as a graphical representation using the "rms" package (R software version 4.0.2, http://www.r-project.org). Student's *t*-test or Mann-Whitney U test was used to compare the continuous variables. Fisher's exact test or Pearson's chi-squared test was used to compare the categorical variables. $P < 0.05$ indicated statistical significance.

RESULTS

Patient characteristics

The patients were divided into two groups according to the histopathological results: MVI+ group and the MVI- group. Among 113 HCCs, 73 had MVI (4 patients had no HBP images), while 40 had no MVI (4 patients had no HBP images). The patients' clinical and radiological characteristics are listed in Tables 1 and 2, respectively. There were statistically significant differences in alpha-fetoprotein (AFP), pathologic grade, maximum tumor diameter (MTD), arterial rim enhancement, tumor margin, and peritumoral hypointensity in the HBP between the MVI+ and MVI- groups ($P < 0.050$).

Table 2 Comparison of different imaging features according to microvascular invasion

MRI feature	MVI+ (*n* = 73)	MVI- (*n* = 40)	*P* value
MTD (cm)[1]	7.23 ± 4.30	3.80 ± 2.43	< 0.001
Arterial rim enhancement (%)			0.002
Absent	37 (50.7)	32 (80)	
Present	36 (49.3)	8 (20)	
Arterial peritumoral enhancement (%)			0.134
Absent	53 (72.6)	34 (85)	
Present	20 (27.4)	6 (15)	
Tumor margin (%)			0.004
Smooth	36 (49.3)	31 (77.5)	
Non-smooth	37 (50.7)	9 (22.5)	
Radiological capsule (%)			0.303
Absent	19 (26.0)	7 (17.5)	
Present	54 (74.0)	33 (82.5)	
Tumor hypointensity in the HBP (%)			0.336
Absent	2 (2.9)	3 (8.3)	
Present	67 (97.1)	33 (91.7)	
Peritumoral hypointensity in the HBP (%)			0.016
Absent	17 (24.6)	34 (94.4)	
Present	52 (75.4)	2 (5.6)	

[1]Data are the mean ± SD.

There were eight patients who had no HBP images. HBP: Hepatobiliary phase; MVI: Microvascular invasion; MTD: Maximum tumor diameter; MRI: Magnetic resonance imaging.

Radiomic analysis

For the MVI+ and MVI- patients, the values of MDFs resulting from the LDA model under B11 analysis were significantly different between the two groups ($P < 0.001$). The analysis of MDF values with ROCs generated an AUC of 0.82 [95% confidence interval (CI): 0.77-0.87] for T1WI; 0.77 (95%CI: 0.72-0.83) for T2WI; 0.84 (95%CI: 0.80-0.88) for AP; 0.85 (95%CI: 0.81-0.90) for PVP; 0.84 (95%CI: 0.79-0.88) for EP; and 0.83 (95%CI: 0.78-0.87) for HBP images. Cutoff values of -1.38×10^{-3} (T1WI), 4.73×10^{-3} (T2WI), 1.97×10^{-2} (AP), 4.17×10^{-3} (PVP), 2.25×10^{-2} (EP), and 4.30×10^{-4} (HBP) were obtained with corresponding high sensitivities and specificities (T1WI: 78% and 78%; T2WI: 59% and 80%; AP: 87% and 66%; PVP: 67% and 90%; EP: 68% and 85%; HBP: 76% and 79%, respectively). The predictive power (AUC) of MDFs derived from the radiomics analysis was better than that of all other histogram parameters (T1WI: 0.52-0.68; T2WI: 0.53-0.70; AP: 0.54-0.69; PVP: 0.50-0.74; EP: 0.51-0.74; HBP: 0.52-0.65) (Tables 3 and 4). The MRI images of four MVI+ and MVI- cases in the AP and PVP are presented, which show similar histogram features but different MDFs (Figure 4 and Supplementary Table 1).

Association of MDFs and patient characteristics with microvascular invasion

We excluded the patients who had no HBP images. MDF values were derived from the largest cross-sectional area of images for univariate analysis. Univariate analysis showed that MDF_{T1WI} greater than -1.38×10^{-3} [odds ratio (OR) = 11.2000, 95%CI: 4.346-28.861; $P < 0.001$], MDF_{T2WI} greater than 4.73×10^{-3} (OR = 6.066, 95%CI: 2.334-15.765; $P < 0.001$), MDF_{AP} greater than 1.97×10^{-2} (OR = 8.552, 95%CI: 2.967-24.650; $P < 0.001$), MDF_{PVP} less than 4.17×10^{-3} (OR = 0.050, 95%CI: 0.017-0.143; $P < 0.001$), MDF_{EP} less than 2.25×10^{-2} (OR = 0.095, 95%CI: 0.037-0.244; $P < 0.001$), and MDF_{HBP} greater than 4.30×10^{-4} (OR = 8.800, 95%CI: 3.222-24.032; $P < 0.001$) were important risk factors related to the presence of MVI. Among patient characteristics, univariate analysis showed that MTD (OR = 1.351, 95%CI: 1.146–1.593; $P < 0.001$), AFP level (OR = 3.818, 95%CI: 1.357–10.605; $P = 0.028$), arterial rim enhancement (present *vs* absent, OR = 5.683, 95%CI: 1.977–16.340; $P = 0.001$), tumor margin (non-smooth *vs* smooth, OR = 4.024, 95%CI: 1.555–10.414; $P = 0.004$), and peritumoral hypointensity in the HBP (present *vs* absent, OR = 52.000, 95%CI: 11.287–239.569; $P < 0.001$) were significant risk factors associated with the presence of MVI

Table 3 Receiver operating characteristic results of radiomic analysis based on most discriminant factors in arterial phase and histogram parameters to discriminate between microvascular invasion+ and microvascular invasion- groups

	MVI (-)	MVI (+)	AUC	Sensitivity	Specificity	*P* value	Cut-off value
MDF	(-4.80 ± 6.14) × 10^{-2}	(2.63 ± 4.74) × 10^{-2}	0.84 (0.80-0.88)	87%	66%	< 0.001	1.97 × 10^{-2}
Histogram parameters							
Mean	(1.27 ± 0.28) × 10^{2}	(1.09 ± 0.26) × 10^{2}	0.68 (0.63-0.74)	78%	52%	< 0.001	1.06 × 10^{2}
Variance	(5.28 ± 4.24) × 10^{2}	(4.57 ± 3.21) × 10^{2}	0.54 (0.48-0.61)	68%	45%	0.204	3.32 × 10^{2}
Skewness	(-9.71 ± 58.46) × 10^{-2}	(2.52 ± 5.79) × 10^{-1}	0.68 (0.62-0.74)	76%	58%	< 0.001	1.30 × 10^{-1}
Kurtosis	(-5.24 ± 91.73) × 10^{-2}	(4.06 ± 11.19) × 10^{-1}	0.60 (0.53-0.66)	90%	25%	0.004	-5.96 × 10^{-1}
Perc.01%	(0.80 ± 0.20) × 10^{2}	(0.68 ± 0.20) × 10^{2}	0.68 (0.62-0.74)	78%	50%	< 0.001	64.5
Perc.10%	(0.99 ± 0.23) × 10^{2}	(0.84 ± 0.22) × 10^{2}	0.68 (0.62-0.74)	96%	32%	< 0.001	69.5
Perc.50%	(1.28 ± 0.30) × 10^{2}	(1.08 ± 0.27) × 10^{2}	0.69 (0.63-0.74)	76%	47%	< 0.001	105.5
Perc.90%	(1.54 ± 0.34) × 10^{2}	(1.35 ± 0.31) × 10^{2}	0.65 (0.59-0.71)	57%	70%	< 0.001	148.5
Perc.99%	(1.73 ± 0.39) × 10^{2}	(1.57 ± 0.35) × 10^{2}	0.62 (0.55-0.68)	48%	74%	< 0.001	177.5

AUC: Area under the receiver operating characteristic curve; MDF: Most discriminant factor; MVI: Microvascular invasion.

Table 4 Receiver operating characteristic results of radiomic analysis based on most discriminant factors in portal venous phase and histogram parameters to discriminate between microvascular invasion+ and microvascular invasion- groups

	MVI (-)	MVI (+)	AUC	Sensitivity	Specificity	*P* value	Cut-off value
MDF	(7.84 ± 9.26) × 10^{-3}	(-4.30 ± 7.00) × 10^{-3}	0.85 (0.81-0.90)	67%	90%	< 0.001	4.17 × 10^{-3}
Histogram parameters							
Mean	(1.24 ± 0.24) × 10^{2}	(1.08 ± 0.24) × 10^{2}	0.69 (0.63-0.75)	78%	54%	< 0.001	106.6
Variance	(3.07 ± 4.11) × 10^{2}	(4.30 ± 3.59) × 10^{2}	0.67 (0.61-0.74)	80%	50%	< 0.001	165.9
Skewness	(1.93 ± 6.11) × 10^{-1}	(1.87 ± 5.85) × 10^{-1}	0.50 (0.44-0.57)	16%	88%	0.09	7.76 × 10^{-1}
Kurtosis	(0.60 ± 1.20)	(0.62 ± 1.19)	0.51 (0.44-0.57)	57%	51%	0.787	1.62 × 10^{-1}
Perc.01%	(91.84 ± 30.33)	(67.16 ± 24.85)	0.74 (0.68-0.80)	50%	90%	< 0.001	101.5
Perc.10%	(1.06 ± 0.29) × 10^{2}	(0.84 ± 0.25) × 10^{2}	0.72 (0.67-0.78)	56%	81%	< 0.001	107.5
Perc.50%	(1.25 ± 0.24) × 10^{2}	(1.07 ± 0.24) × 10^{2}	0.69 (0.64-0.75)	78%	55%	< 0.001	106.5
Perc.90%	(1.44 ± 0.27) × 10^{2}	(1.32 ± 0.27) × 10^{2}	0.62 (0.56-0.68)	63%	61%	< 0.001	137.5
Perc.99%	(1.61 ± 0.31) × 10^{2}	(1.56 ± 0.34) × 10^{2}	0.55 (0.49-0.61)	35%	77%	0.179	176.5

AUC: Area under the receiver operating characteristic curve; MDF: Most discriminant factor; MVI: Microvascular invasion.

(Table 5).

Multivariate analysis of MDF values and patient characteristics with microvascular invasion

Multivariate analysis of the above 11 significant parameters showed that only MDF_{AP} (> 1.97 × 10^{-2} *vs* ≤ 1.97 × 10^{-2}, OR = 7.654, 95%CI: 1.860-31.501; P = 0.005), MDF_{PVP} (> 4.17 × 10^{-3} *vs* ≤ 4.17 × 10^{-3}, OR = 0.182, 95%CI: 0.047-0.705; P = 0.014), and peritumoral hypointensity in the HBP (present *vs* absent, OR = 37.098, 95%CI: 6.861-200.581; P < 0.001) were independent predictors related to the presence of MVI (Figure 5).

Table 5 Univariate analysis of risk factors for most discriminant factors and patient characteristic

Variable	OR	95%CI	*P* value
MDF_{T1}	11.200	4.346-28.861	< 0.001[a]
MDF_{T2}	6.066	2.334-15.765	< 0.001[a]
MDF_{AP}	8.552	2.967-24.650	< 0.001[a]
MDF_{PVP}	0.050	0.017-0.143	< 0.001[a]
MDF_{EP}	0.095	0.037-0.244	< 0.001[a]
MDF_{HBP}	8.800	3.222-24.032	< 0.001[a]
MTD	1.351	1.146-1.593	< 0.001[a]
AFP	3.818	1.375-10.605	0.028[a]
Pathologic grade			0.105
Arterial rim enhancement	5.683	1.977-16.340	0.001[a]
Arterial peritumoral enhancement			0.215
Tumor margin	4.024	1.555-10.414	0.004[a]
Radiological capsule			0.275
Tumor hypointensity in HBP			0.215
Peritumoral hypointensity in HBP	52.000	11.287-239.569	< 0.001[a]

[a]*P* < 0.05, statistically significant results from logistic regression analysis. Variables with [a]*P* < 0.05 in univariate logistic regression analysis were applied to a multivariate logistic regression analysis.

MDF: Most discriminant factor; AFP: Alpha-fetoprotein; AP: Arterial phase; CI: Confidence interval; EP: Equilibrium phase; HBP: Hepatobiliary phase; MTD: Maximum tumor diameter; OR: Odds ratio; PVP: Portal venous phase.

The risk scores for individual patients based on the final discriminant model were calculated using the following formula: Logit (P) = −4.612 + 3.614 × peritumoral hypointensity on HBP (absent = 0, present = 1) + 2.035 × MDF_{AP} (≤ 1.97×10^{-2} *vs* > 1.97×10^{-2}, ≤ 1.97×10^{-2} = 0, > 1.97×10^{-2} = 1) - 1.876 × MDF_{PVP} (≤ 4.17×10^{-3} *vs* > 4.17×10^{-3}, ≤ 4.17×10^{-3} = 0, > 4.17×10^{-3} = 1). The probabilities of MVI were calculated by the formula [P = e Logit (P)/1 + e Logit (P)].

The AUC of the final model was 0.939 (95%CI: 0.893-0.984; standard error: 0.023) and the optimal cutoff value was 0.595881 ≈ 0.60 (specificity: 89%; sensitivity: 90%; Youden's index: 0.788) (Figure 6A). The result of internal five-fold cross-validation (AUC: 0.912; 95%CI: 0.841-0.959; standard error: 0.0298) also showed favorable predictive efficacy (Figure 6A). The independent predictive factors were integrated into a nomogram by the multivariate logistic regression analysis (Figure 6B).

Comparison of area under the receiver operating characteristic curve values of MDF values and imaging features

We generated the ROC curves of MDF_{AP} and $MDF_{PVP,}$ respectively, which were independent predictors. The ROC curves of imaging features which were significantly different were also generated alone. The results were compared using the Delong test. The MDF_{AP} and MDF_{PVP} had significantly higher AUCs than MTDs, arterial rim enhancement, and tumor margin ($P < 0.05$; Supplementary Table 2). However, there were no differences in AUCs among MDF_{AP}, MDF_{PVP}, and peritumoral hypointensity in the HBP ($P > 0.05$; Supplementary Table 1). Comparison of ROC curves is shown in Figure 6C.

DISCUSSION

MVI indicates the invasiveness of HCC and poor prognosis[2,3]. Therefore, the pre-operative prediction of MVI is an important factor for assessing long-term patient survival and treatment optimization. The quantification of MRI images by radiomic analysis can characterize the heterogeneity of tumor and has demonstrated previous success in reflecting histological subtype[33,34]. In the present study, through the analysis of the top 30 parameters in each sequence, an overall discriminator, MDF, was generated with the LDA model, providing better prediction ability for MVI than the histogram features.

Our study showed a high sensitivity of MDF values from radiomic analysis on preoperative Gd-enhanced MRI images and/or specificity in distinguishing between MVI+ and MVI-. The AUCs of MDF values of six sequences, all of which were more than 0.75, outperformed those of all histogram

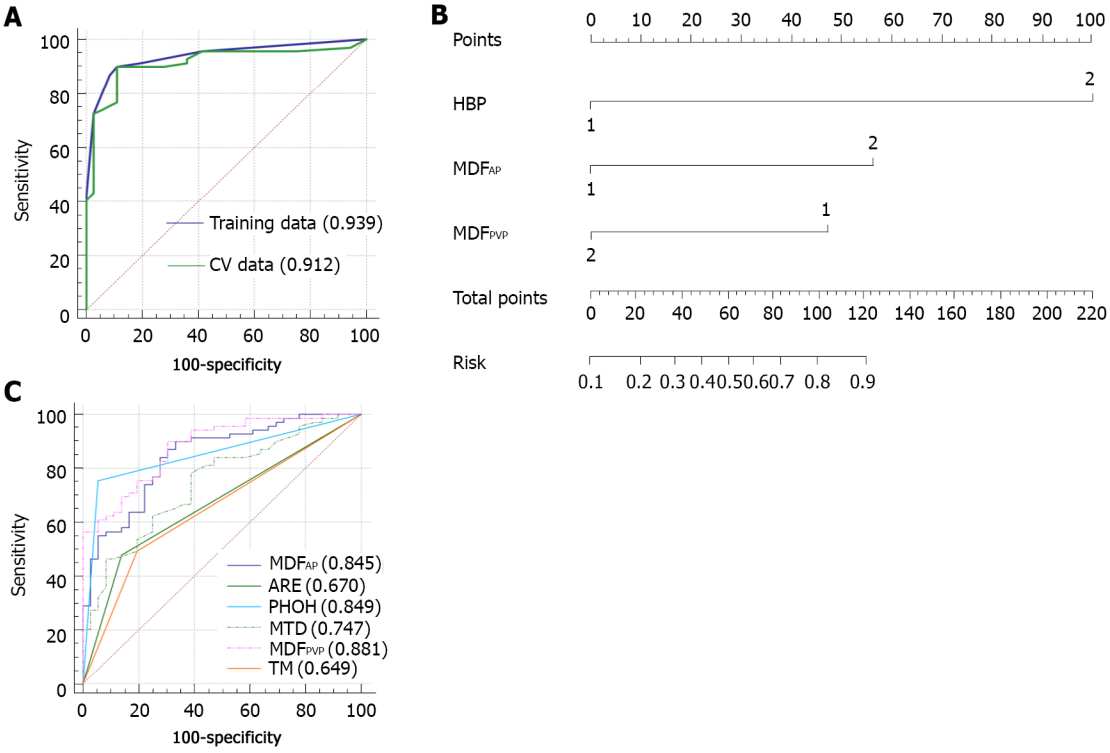

DOI: 10.3748/wjg.v28.i24.2733

Figure 6 Area under the receiver operating characteristic curve of the final model. A: Receiver operating characteristic (ROC) curves of the selected model and the ROC curve of the 5-fold cross-validation; B: Nomogram of the integrated model. Hepatobiliary phase (HBP) means peritumoral hypointensity in the HBP, most discriminant factor (MDF)$_{AP}$ means the MDF of the arterial phase, and MDF$_{PVP}$ means the MDF of the portal venous phase; C: Comparison of ROC curves for prediction of microvascular invasion. The area under the ROC curve (AUC) was largest for the MDF$_{PVP}$ alone (AUC = 0.881). ARE: Arterial rim enhancement; MTD: Maximum tumor diameter; PHOH: Peritumoral hypointensity in the HBP; TM: Tumor margin.

parameters and imaging features. The MDF values of AP and PVP images had significantly higher AUCs than most of imaging features. MDF values could provide additional information useful for clinical management decisions. Moreover, MaZda software can be easily used for general clinicians without additional requirement of expertise, easily serving as a potential powerful tool in preoperative prediction of MVI.

LDA has been used in radiomics studies recently[35]. Han *et al*[35] found that LDA and support vector machine achieved optimal performance when compared with multiple machine learning methods[35]. In our study, among the LDA models based on various sequences, MDF$_{AP}$ and MDF$_{PVP}$ were significant independent factors for the prediction of MVI, and showed satisfactory predictive efficacy with an AUC greater than 0.80. Histogram parameters have been used in quantitative analysis of MVI in clinical studies[19,20]. Li *et al*[19] performed histogram analysis of intravoxel incoherent motion and the best parameter provided a sensitivity of 81% and specificity of 85%[19]. It was based on whole tumor volume, but only 41 patients were enrolled. Wang *et al*[20] used computational quantitative measures based on the maximum cross-sectional area to predict MVI of small HCC, but only in HBP images[20]; the AUC, sensitivity, and specificity were 0.91, 0.87, and 0.80, respectively. In our study, the radiomic analysis-based MDF outperformed each individual histogram parameter in predicting the presence of MVI. Therefore, we considered that MDFs on the basis of LDA model that contained more comprehensive information could evaluate the Gd-enhanced MR images and determine MVI status better than histogram analysis alone.

Multivariate analysis of the 11 risk factors identified in the univariate analysis found that only peritumoral hypointensity in HCCs in the HBP, MDF$_{PVP}$, and MDF$_{AP}$ were independent predictors of MVI. Pathologically, MVI is usually found in the small portal vein and hepatic artery[4]. It may be detected in the small liver lymphatic vessels. But it is mostly found in small branches of the portal vein. This may explain why the MDF$_{PVP}$ and MDF$_{AP}$ were independent predictors of MDF values in the model that predicted MVI. The MDF$_{PVP}$ whose OR was less than 1 may be a protective factor, which means that the higher the MDF$_{PVP}$, the less possible the presence of MVI. MVI may affect the biological functions of the canalicular transporter multidrug resistance-associated protein 2 or the organic anion transporting peptides, both of which lead to the elimination of gadoxetate disodium. That may be the reason why peritumoral hypointensity appeared in HCCs in the HBP[12]. The OR of peritumoral hypointensity in the HBP was quite high, which may result from relatively small sample size.

It has been reported that MR findings including arterial peritumoral enhancement and non-smooth tumor margin were independent predictors associated with the presence of MVI or indicated the association between the hypointensity of HCCs in HBP images and a higher frequency of MVI[12,17], which is not consistent with our study. One possible reason for the inconsistence may be the differences between study populations, as all patients enrolled in that study had a single HCC with a diameter ≤ 5 cm. The inherent and technical inconsistencies between the observers in two studies may also account for the incompatible results. Arterial rim enhancement can predict biological characters of HCCs, including MVI, rapid progression, and early recurrence[26,36]. Our study showed that rim enhancement in the AP was not an independent predictor of MVI, and the reason may be that rim enhancement in AP is uncommon in HCC but more often seen in mass-forming cholangiocarcinoma or metastasis[37].

There are some limitations in this study. First, a selection bias may exist due to the retrospective study. Second, the radiomic analysis was performed only on the largest cross-sectional area and two adjacent images of the tumor. There may be information loss compared to whole tumors. In spite of this, our results showed excellent discriminative efficacy between the MVI+ and MVI- groups. Third, different MVI grading indicates a decreasing gradient of overall survival and time to early recurrence, which was not analyzed in the MVI+ group due to the small sample size. Finally, this study was performed at only one institution, causing the sample size small relative to the number of variables. Further multicenter, prospective studies are needed to validate the results of this study.

CONCLUSION

In conclusion, radiomic analysis based on preoperative Gd-enhanced MR images may be feasible for predicting MVI of HCC. Upon the application of MRI findings and radiomic variables in our model, the diagnostic prediction of MVI showed a high specificity and sensitivity, indicating that this method is a useful tool for clinicians in treatment decision-making.

ARTICLE HIGHLIGHTS

Research background

The prognosis of hepatocellular carcinoma (HCC) remains poor and relapse occurs in more than half of the patients within 2 years after hepatectomy. Microvascular invasion (MVI) is one of the potential predictors of recurrence. MVI is defined as the appearance of tumor cells in smaller vessels inside the liver which include small portal vein, and small lymphatic vessels or hepatic arteries. Accurate preoperative prediction of MVI is potentially beneficial to the optimization of treatment planning.

Research motivation

There have been some studies to preoperatively predict MVI in terms of serum markers, radiological features, or imaging techniques. However, the levels of serum markers are instable and likely to be affected by other diseases, and the imaging characteristics are evaluated subjectively and lack of conformance between observers. Thus, a more reliable biomarker is needed for preoperative prediction of MVI.

Research objectives

The aim of this study was to develop a radiomic analysis model based on pre-operative magnetic resonance imaging (MRI) data to predict MVI in HCC.

Research methods

A total of 113 patients recruited to this study have been diagnosed as having HCC with histological confirmation, among whom, 73 were found to have MVI and 40 were not. All the patients received preoperative examination by Gd-enhanced MRI and then curative hepatectomy. We manually delineated the tumor lesion on the largest cross-sectional area of the tumor and the two adjacent images on MRI. Quantitative analyses included most discriminant factors (MDFs) developed using a linear discriminant analysis algorithm and histogram analysis *via* MaZda software. Independent significant variables of clinical and radiological features and MDFs for the prediction of MVI were estimated and a discriminant model was established by univariate and multivariate logistic regression analysis. Prediction ability of the above-mentioned parameters or model was then evaluated by receiver operating characteristic (ROC) curve analysis, and five-fold cross-validation was applied *via* R software.

Research results

The area under the ROC curve of the MDF (0.77-0.85) outperformed the histogram parameters (0.51-0.74). After multivariate analysis, MDF values of the arterial and portal venous phase, and peritumoral

hypointensity in the hepatobiliary phase were identified to be independent predictors of MVI ($P < 0.05$). The area under the ROC curve (AUC) value of the model was 0.939. The result of internal five-fold cross-validation (AUC: 0.912) also showed favorable predictive efficacy.

Research conclusions

Noninvasive MRI radiomic model based on MDF values and imaging biomarkers may be useful to make preoperative prediction of MVI in patients with primary HCC.

Research perspectives

We believe that noninvasive radiomic models based on pre-operative MRI data have potential to be widely used in clinical fields.

ACKNOWLEDGEMENTS

We thank the radiographers at the First Affiliated Hospital of Fujian Medical University for scanning the patients and data collections in this study.

FOOTNOTES

Author contributions: Li YM, Zhu YM, and Cao DR worked out the conceptualization; Li YM, Cao DR, and Zhu YM did the methodology; Zhu YM and Yan C analyzed, collected, and interpreted the data; Li YM and Cao DR contributed to study supervision; all authors edited and reviewed the manuscript, and have read and approved the final manuscript.

Supported by Joint Funds for the Innovation of Science and Technology, Fujian Province (CN), No. 2019Y9125.

Institutional review board statement: This study was reviewed and approved by the Ethics Committee of the First Affiliated Hospital of Fujian Medical University.

Informed consent statement: This study was approved by the institutional review board of our institution. The requirement for written informed consent was waived for this retrospective study.

Conflict-of-interest statement: The authors declare that the research was conducted in the absence of any commercial or financial relationships that could be construed as a potential conflict of interest.

Data sharing statement: No additional data are available.

Country/Territory of origin: China

ORCID number: Yue-Ming Li 0000-0002-3669-568X; Yue-Min Zhu 0000-0001-9630-0160; Lan-Mei Gao 0000-0002-6032-6884; Ze-Wen Han 0000-0002-0146-8583; Xiao-Jie Chen 0000-0003-4521-3803; Chuan Yan 0000-0003-4106-8995; Rong-Ping Ye 0000-0001-7867-9752; Dai-Rong Cao 0000-0002-0051-3143.

S-Editor: Fan JR
L-Editor: Wang TQ
P-Editor: Fan JR

REFERENCES

1 **Llovet JM**, Kelley RK, Villanueva A, Singal AG, Pikarsky E, Roayaie S, Lencioni R, Koike K, Zucman-Rossi J, Finn RS. Hepatocellular carcinoma. *Nat Rev Dis Primers* 2021; **7**: 6 [PMID: 33479224 DOI: 10.1038/s41572-020-00240-3]
2 **Zhang X**, Li J, Shen F, Lau WY. Significance of presence of microvascular invasion in specimens obtained after surgical treatment of hepatocellular carcinoma. *J Gastroenterol Hepatol* 2018; **33**: 347-354 [PMID: 28589639 DOI: 10.1111/jgh.13843]
3 **Erstad DJ**, Tanabe KK. Prognostic and Therapeutic Implications of Microvascular Invasion in Hepatocellular Carcinoma. *Ann Surg Oncol* 2019; **26**: 1474-1493 [PMID: 30788629 DOI: 10.1245/s10434-019-07227-9]

4 **Gouw AS**, Balabaud C, Kusano H, Todo S, Ichida T, Kojiro M. Markers for microvascular invasion in hepatocellular carcinoma: where do we stand? *Liver Transpl* 2011; **17** Suppl 2: S72-S80 [PMID: 21714066 DOI: 10.1002/lt.22368]

5 **European Association for the Study of the Liver**. EASL Clinical Practice Guidelines: Management of hepatocellular carcinoma. *J Hepatol* 2018; **69**: 182-236 [PMID: 29628281 DOI: 10.1016/j.jhep.2018.03.019]

6 **Feng LH**, Dong H, Lau WY, Yu H, Zhu YY, Zhao Y, Lin YX, Chen J, Wu MC, Cong WM. Novel microvascular invasion-based prognostic nomograms to predict survival outcomes in patients after R0 resection for hepatocellular carcinoma. *J Cancer Res Clin Oncol* 2017; **143**: 293-303 [PMID: 27743138 DOI: 10.1007/s00432-016-2286-1]

7 **Han J**, Li ZL, Xing H, Wu H, Zhu P, Lau WY, Zhou YH, Gu WM, Wang H, Chen TH, Zeng YY, Wu MC, Shen F, Yang T. The impact of resection margin and microvascular invasion on long-term prognosis after curative resection of hepatocellular carcinoma: a multi-institutional study. *HPB (Oxford)* 2019; **21**: 962-971 [PMID: 30718183 DOI: 10.1016/j.hpb.2018.11.005]

8 **Lei Z**, Li J, Wu D, Xia Y, Wang Q, Si A, Wang K, Wan X, Lau WY, Wu M, Shen F. Nomogram for Preoperative Estimation of Microvascular Invasion Risk in Hepatitis B Virus-Related Hepatocellular Carcinoma Within the Milan Criteria. *JAMA Surg* 2016; **151**: 356-363 [PMID: 26579636 DOI: 10.1001/jamasurg.2015.4257]

9 **Zheng J**, Seier K, Gonen M, Balachandran VP, Kingham TP, D'Angelica MI, Allen PJ, Jarnagin WR, DeMatteo RP. Utility of Serum Inflammatory Markers for Predicting Microvascular Invasion and Survival for Patients with Hepatocellular Carcinoma. *Ann Surg Oncol* 2017; **24**: 3706-3714 [PMID: 28840521 DOI: 10.1245/s10434-017-6060-7]

10 **Hu H**, Zheng Q, Huang Y, Huang XW, Lai ZC, Liu J, Xie X, Feng ST, Wang W, Lu M. A non-smooth tumor margin on preoperative imaging assesses microvascular invasion of hepatocellular carcinoma: A systematic review and meta-analysis. *Sci Rep* 2017; **7**: 15375 [PMID: 29133822 DOI: 10.1038/s41598-017-15491-6]

11 **Huang M**, Liao B, Xu P, Cai H, Huang K, Dong Z, Xu L, Peng Z, Luo Y, Zheng K, Peng B, Li ZP, Feng ST. Prediction of Microvascular Invasion in Hepatocellular Carcinoma: Preoperative Gd-EOB-DTPA-Dynamic Enhanced MRI and Histopathological Correlation. *Contrast Media Mol Imaging* 2018; **2018**: 9674565 [PMID: 29606926 DOI: 10.1155/2018/9674565]

12 **Lee S**, Kim SH, Lee JE, Sinn DH, Park CK. Preoperative gadoxetic acid-enhanced MRI for predicting microvascular invasion in patients with single hepatocellular carcinoma. *J Hepatol* 2017; **67**: 526-534 [PMID: 28483680 DOI: 10.1016/j.jhep.2017.04.024]

13 **Chamming's F**, Ueno Y, Ferré R, Kao E, Jannot AS, Chong J, Omeroglu A, Mesurolle B, Reinhold C, Gallix B. Features from Computerized Texture Analysis of Breast Cancers at Pretreatment MR Imaging Are Associated with Response to Neoadjuvant Chemotherapy. *Radiology* 2018; **286**: 412-420 [PMID: 28980886 DOI: 10.1148/radiol.2017170143]

14 **Yang L**, Gu D, Wei J, Yang C, Rao S, Wang W, Chen C, Ding Y, Tian J, Zeng M. A Radiomics Nomogram for Preoperative Prediction of Microvascular Invasion in Hepatocellular Carcinoma. *Liver Cancer* 2019; **8**: 373-386 [PMID: 31768346 DOI: 10.1159/000494099]

15 **He B**, Dong D, She Y, Zhou C, Fang M, Zhu Y, Zhang H, Huang Z, Jiang T, Tian J, Chen C. Predicting response to immunotherapy in advanced non-small-cell lung cancer using tumor mutational burden radiomic biomarker. *J Immunother Cancer* 2020; **8** [PMID: 32636239 DOI: 10.1136/jitc-2020-000550]

16 **Lambin P**, Leijenaar RTH, Deist TM, Peerlings J, de Jong EEC, van Timmeren J, Sanduleanu S, Larue RTHM, Even AJG, Jochems A, van Wijk Y, Woodruff H, van Soest J, Lustberg T, Roelofs E, van Elmpt W, Dekker A, Mottaghy FM, Wildberger JE, Walsh S. Radiomics: the bridge between medical imaging and personalized medicine. *Nat Rev Clin Oncol* 2017; **14**: 749-762 [PMID: 28975929 DOI: 10.1038/nrclinonc.2017.141]

17 **Xu X**, Zhang HL, Liu QP, Sun SW, Zhang J, Zhu FP, Yang G, Yan X, Zhang YD, Liu XS. Radiomic analysis of contrast-enhanced CT predicts microvascular invasion and outcome in hepatocellular carcinoma. *J Hepatol* 2019; **70**: 1133-1144 [PMID: 30876945 DOI: 10.1016/j.jhep.2019.02.023]

18 **Chong HH**, Yang L, Sheng RF, Yu YL, Wu DJ, Rao SX, Yang C, Zeng MS. Multi-scale and multi-parametric radiomics of gadoxetate disodium-enhanced MRI predicts microvascular invasion and outcome in patients with solitary hepatocellular carcinoma ≤ 5 cm. *Eur Radiol* 2021; **31**: 4824-4838 [PMID: 33447861 DOI: 10.1007/s00330-020-07601-2]

19 **Li H**, Zhang J, Zheng Z, Guo Y, Chen M, Xie C, Zhang Z, Mei Y, Feng Y, Xu Y. Preoperative histogram analysis of intravoxel incoherent motion (IVIM) for predicting microvascular invasion in patients with single hepatocellular carcinoma. *Eur J Radiol* 2018; **105**: 65-71 [PMID: 30017300 DOI: 10.1016/j.ejrad.2018.05.032]

20 **Wang X**, Zhang Z, Zhou X, Zhang Y, Zhou J, Tang S, Liu Y, Zhou Y. Computational quantitative measures of Gd-EOB-DTPA enhanced MRI hepatobiliary phase images can predict microvascular invasion of small HCC. *Eur J Radiol* 2020; **133**: 109361 [PMID: 33120240 DOI: 10.1016/j.ejrad.2020.109361]

21 **Szczypiński PM**, Strzelecki M, Materka A, Klepaczko A. MaZda--a software package for image texture analysis. *Comput Methods Programs Biomed* 2009; **94**: 66-76 [PMID: 18922598 DOI: 10.1016/j.cmpb.2008.08.005]

22 **Strzelecki M**, Szczypinski P, Materka A, Klepaczko A. A software tool for automatic classification and segmentation of 2D/3D medical images. *Nucl Instrum Methods Phys Res* 2013; **702**: 137-140 [DOI: 10.1016/j.nima.2012.09.006]

23 **Yan PF**, Yan L, Hu TT, Xiao DD, Zhang Z, Zhao HY, Feng J. The Potential Value of Preoperative MRI Texture and Shape Analysis in Grading Meningiomas: A Preliminary Investigation. *Transl Oncol* 2017; **10**: 570-577 [PMID: 28654820 DOI: 10.1016/j.tranon.2017.04.006]

24 **Vallières M**, Freeman CR, Skamene SR, El Naqa I. A radiomics model from joint FDG-PET and MRI texture features for the prediction of lung metastases in soft-tissue sarcomas of the extremities. *Phys Med Biol* 2015; **60**: 5471-5496 [PMID: 26119045 DOI: 10.1088/0031-9155/60/14/5471]

25 **Brown AM**, Nagala S, McLean MA, Lu Y, Scoffings D, Apte A, Gonen M, Stambuk HE, Shaha AR, Tuttle RM, Deasy JO, Priest AN, Jani P, Shukla-Dave A, Griffiths J. Multi-institutional validation of a novel textural analysis tool for preoperative stratification of suspected thyroid tumors on diffusion-weighted MRI. *Magn Reson Med* 2016; **75**: 1708-1716 [PMID: 25995019 DOI: 10.1002/mrm.25743]

26 **Rhee H**, An C, Kim HY, Yoo JE, Park YN, Kim MJ. Hepatocellular Carcinoma with Irregular Rim-Like Arterial Phase Hyperenhancement: More Aggressive Pathologic Features. *Liver Cancer* 2019; **8**: 24-40 [PMID: 30815393 DOI: 10.1159/000488540]

27 **Kawamura Y**, Ikeda K, Hirakawa M, Yatsuji H, Sezaki H, Hosaka T, Akuta N, Kobayashi M, Saitoh S, Suzuki F, Suzuki Y, Arase Y, Kumada H. New classification of dynamic computed tomography images predictive of malignant characteristics of hepatocellular carcinoma. *Hepatol Res* 2010; **40**: 1006-1014 [PMID: 20887336 DOI: 10.1111/j.1872-034X.2010.00703.x]

28 **Kim H**, Park MS, Choi JY, Park YN, Kim MJ, Kim KS, Choi JS, Han KH, Kim E, Kim KW. Can microvessel invasion of hepatocellular carcinoma be predicted by pre-operative MRI? *Eur Radiol* 2009; **19**: 1744-1751 [PMID: 19247666 DOI: 10.1007/s00330-009-1331-8]

29 **Choi JY**, Lee JM, Sirlin CB. CT and MR imaging diagnosis and staging of hepatocellular carcinoma: part II. Extracellular agents, hepatobiliary agents, and ancillary imaging features. *Radiology* 2014; **273**: 30-50 [PMID: 25247563 DOI: 10.1148/radiol.14132362]

30 **Kitao A**, Matsui O, Yoneda N, Kozaka K, Kobayashi S, Koda W, Gabata T, Yamashita T, Kaneko S, Nakanuma Y, Kita R, Arii S. Hypervascular hepatocellular carcinoma: correlation between biologic features and signal intensity on gadoxetic acid-enhanced MR images. *Radiology* 2012; **265**: 780-789 [PMID: 23175543 DOI: 10.1148/radiol.12120226]

31 **Kim KA**, Kim MJ, Jeon HM, Kim KS, Choi JS, Ahn SH, Cha SJ, Chung YE. Prediction of microvascular invasion of hepatocellular carcinoma: usefulness of peritumoral hypointensity seen on gadoxetate disodium-enhanced hepatobiliary phase images. *J Magn Reson Imaging* 2012; **35**: 629-634 [PMID: 22069244 DOI: 10.1002/jmri.22876]

32 **Roayaie S**, Blume IN, Thung SN, Guido M, Fiel MI, Hiotis S, Labow DM, Llovet JM, Schwartz ME. A system of classifying microvascular invasion to predict outcome after resection in patients with hepatocellular carcinoma. *Gastroenterology* 2009; **137**: 850-855 [PMID: 19524573 DOI: 10.1053/j.gastro.2009.06.003]

33 **Li Y**, Yan C, Weng S, Shi Z, Sun H, Chen J, Xu X, Ye R, Hong J. Texture analysis of multi-phase MRI images to detect expression of Ki67 in hepatocellular carcinoma. *Clin Radiol* 2019; **74**: 813.e19-813.e27 [PMID: 31362887 DOI: 10.1016/j.crad.2019.06.024]

34 **Zhang S**, Chiang GC, Magge RS, Fine HA, Ramakrishna R, Chang EW, Pulisetty T, Wang Y, Zhu W, Kovanlikaya I. Texture analysis on conventional MRI images accurately predicts early malignant transformation of low-grade gliomas. *Eur Radiol* 2019; **29**: 2751-2759 [PMID: 30617484 DOI: 10.1007/s00330-018-5921-1]

35 **Han Y**, Ma Y, Wu Z, Zhang F, Zheng D, Liu X, Tao L, Liang Z, Yang Z, Li X, Huang J, Guo X. Histologic subtype classification of non-small cell lung cancer using PET/CT images. *Eur J Nucl Med Mol Imaging* 2021; **48**: 350-360 [PMID: 32776232 DOI: 10.1007/s00259-020-04771-5]

36 **Kierans AS**, Leonardou P, Hayashi P, Brubaker LM, Elazzazi M, Shaikh F, Semelka RC. MRI findings of rapidly progressive hepatocellular carcinoma. *Magn Reson Imaging* 2010; **28**: 790-796 [PMID: 20427139 DOI: 10.1016/j.mri.2010.03.005]

37 **Zou X**, Luo Y, Morelli JN, Hu X, Shen Y, Hu D. Differentiation of hepatocellular carcinoma from intrahepatic cholangiocarcinoma and combined hepatocellular-cholangiocarcinoma in high-risk patients matched to MR field strength: diagnostic performance of LI-RADS version 2018. *Abdom Radiol (NY)* 2021; **46**: 3168-3178 [PMID: 33660040 DOI: 10.1007/s00261-021-02996-y]

Published by **Baishideng Publishing Group Inc**
7041 Koll Center Parkway, Suite 160, Pleasanton, CA 94566, USA
Telephone: +1-925-3991568
E-mail: bpgoffice@wjgnet.com
Help Desk: https://www.f6publishing.com/helpdesk
https://www.wjgnet.com